A simple panel zone model for linear analysis of steel moment frames

Hamed Saffari* and Esmaeil Morshedi

*Department of Civil Engineering, Faculty of Engineering, Shahid Bahonar University of Kerman, 22 Bahman Blvd,
P.O. Box 76175-133, Kerman, Iran*

Abstract. Consideration of the panel zone (PZ) deformations in the analysis of steel moment frames (SMFs) has a substantial effect on structural response. One way to include the PZ effect on the structural response is Krawinkler's PZ model, which is one of the best and conventional models. However, modeling of Krawinkler's PZ model has its complexity, and finding an alternative procedure for PZ modeling is of interest. In this study, an efficient model is proposed to simplify Krawinkler's PZ model into an Adjusted Rigid-End Zone (AREZ). In this way, the rigid-end-zone dimensions of the beam and column elements are defined through an appropriate rigid-end-zone factor. The dimensions of this region depend on the PZ stiffness, beam(s) and columns' specifications, and connection joint configuration. Thus, to obtain a relationship for the AREZ model, which yields the dimensions of the rigid-end zone, the story drift of an SMF with Krawinkler's PZ model is equalized with the story drift of the same structure with the AREZ model. Then, the degree of accuracy of the resulting relationship is examined in several connections of generic SMFs. Also, in order to demonstrate the applicability of the proposed model in SMFs, several SMFs ranging from 3- to 30-story representing low- to high-rise buildings are examined through linear static and dynamic time history analysis. Furthermore, non-linear dynamic analyses of three SMFs conducted to validate the degree of accuracy of the proposed model in the non-linear analysis of SMFs. Analytical results show that there is considerable conformity between inter-story drift ratio (IDR) results of the SMFs with Krawinkler's PZ model and those of the centerline SMFs with AREZ.

Keywords: rigid-end zone; panel zone deformation; steel moment frames

1. Introduction

Steel moment frames (SMFs) are widely used all over the world. In order to understand the behavior of SMFs, extensive experimental and analytical researches have been conducted. Among these, a considerable number of studies are related to the beam-to-column joints, and more precisely, to the area of column web between beam flanges which is called panel zone (PZ) (Krawinkler *et al*. 1971, Slutter 1982, Kawano 1984, Krawinkler and Mohasseb 1987, Liew and Chen 1995, Castro *et al*. 2005, Adan and Reaveley 2006, Lu *et al*. 2018a, Lu *et al*. 2018b, Lu *et al*. 2017, Kim and Engelhardt 1995, Kim and Engelhardt 2002, Popov *et al*. 1985, Fielding and Huang 1971, Eduardo Nuñez *et al*. 2017, Bertero *et al*. 1973, Lee 1987, Elkady and Lignos 2015, Bayat and Zahrai 2017).

PZ deformations have a significant contribution to the global behavior of SMFs. An analytical study by Kawano (1984) on a 5-story SMF under earthquake excitation showed the PZ shear distortions affect energy dissipation over the height of the structure. Krawinkler and Mohasseb (1987) also examined two SMFs, 7- and 10-story, with different PZ strengths, and it was recommended to design PZ such that both PZ and beams contribute to the energy

dissipation mechanism. Liew and Chen (1995) had shown that the PZ shear deformations increased the drift response, and also decreased the global stiffness and strength of the structures. A study by Castro *et al*. (2005) showed that in the elastic range, the behavior of PZ was generally affected by the shear behavior of the panel area. For these reasons, consideration of PZ behavior is of great importance to the analysis of structures. However, there are sources of uncertainty that lead to inaccurate prediction of the PZ behavior as well as structural responses.

The boundary condition at the connection joint affects both PZ and connection performance. Kim and Engelhardt (1995, 2002) demonstrated that current PZ models are not able to accurately predict the PZ behavior when the columns have flange thickness greater than 2.5 cm. The experimental and numerical investigation by Lu *et al*. (2018a) on the performance of weak-axis steel moment connections revealed that the stress distribution at the connection joint depends on the location of the applied load, whether it is the end of the beam or column. Also, a study on the fracture behavior of reduced beam section (RBS) connections by Lu *et al*. (2018b) showed the significance of the distance between the column face and the beginning of the RBS cut. It was concluded that with increasing this distance, the performance of the connection improves while reducing this distance adversely affects the beam flange groove weld and PZ deformation. The study by Lu *et al*. (2017) on the weak-axis cover-plate steel moment connections showed the PZ behavior is dependent on the loading condition. A parametric study by Bayat and Zahrai

---
∗Corresponding author, Professor
 E-mail: hsaffari@mail.uk.ac.ir
[a]M.Sc. Graduated Student
 E-mail: e.morshedi85@gmail.com

(2017) on the seismic performance of SMFs with semi-rigid connections showed the beneficial effects of such connections on the story drift, roof acceleration, PZ demands, and base shear of the structures. A numerical investigation by Nuñez *et al.* (2017) on the seismic performance of steel moment connections with HSS columns showed that this type of column section prevents stress concentration in the column, specifically in the PZ, and develops significant energy dissipation in the beam. Bertero *et al.* (1973) reviewed the results of experimental data provided by Popov and Stephen (1970) and Krawinkler *et al.* (1971). They mentioned that because the test specimens had medium sizes, a general conclusion for other member sizes should be drawn carefully. Therefore, it can be inferred from the previous studies that the stiffness and strength properties of the current PZ models are representative of a limited number of experimental results.

The presence of column stiffeners and doublar plates increase uncertainty in the PZ response prediction. Popov *et al.* (1985) examined the PZ performance with different types of stiffeners. The research showed that in the column sections with thick flanges, the existence of column stiffeners has a considerable effect on the PZ performance. Fielding and Huang (1971) examined the condition of high shear stress, high axial load, and various types of column stiffeners of the beam-to-column connections under monotonic loading. The test results demonstrated that under different types of column stiffeners and due to varying levels of reserve strength in the PZ area, the prediction of PZ strength and stiffness becomes uncertain. An experimental study by Adan and Reaveley (2006) on the RBS connections showed the beneficial effect of stiffeners on some column sections while they were not effective in some other column sections. Doublar plate is another source of uncertainty. Although Slutter (1982) mentioned some beneficial effects of doublar plates on the PZ behavior, Kim and Engelhardt (1995, 2002) showed that the doublar plates are not as useful as expected in some cases. In addition to the column stiffeners and doublar plates, concrete slab makes the PZ behavior prediction difficult. An experimental study by Lee (1987) and an analytical investigation by Elkady and Lignos (2015) showed a stable hysteresis behavior and high reserve strength of the PZs and an increase in flexural strength in the positive direction of the beams.

Another issue of concern, which is also the most important one, is the PZ modeling approach. Several PZ models have been developed by previous researchers (Fielding and Huang 1971, Krawinkler *et al.* 1971, Wang 1989). Kim and Engelhardt (1995) examined the PZ models of the past researches and compared the results with the results of experimental data. Research showed that in the elastic range, all PZ models are almost similar in behavior. However, in the inelastic range, the applicability of some of the developed models is questionable. Among all models, the model which was developed by Krawinkler *et al.* (1971) showed a reasonable behavior in comparison with test data. This model has been called krawinkler's PZ model (see Fig. 1). Saffari *et al.* (2016) carried out a finite-element parametric study and proposed a mathematical relationship
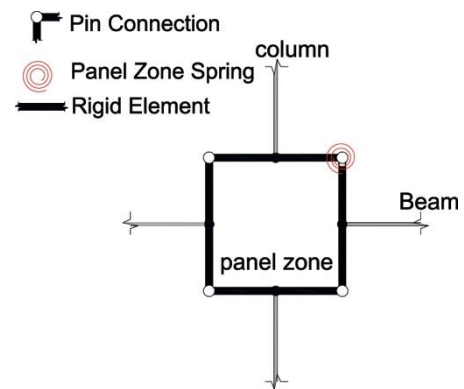

Fig. 1 Krawinkler's PZ model

to consider the PZ deformations of flanged cruciform columns. They showed the importance of the web thicknesses of the column in the PZ deformations. Mansouri and Saffari (2014, 2015) developed a mathematical PZ model to estimate the PZ strength based on several exterior beam-to-column connections considering thick column flanges and axial load effects. The resulting PZ model was calibrated with the results of some finite element simulation of SAC connection specimens. As a result, the proposed PZ model showed a relatively accurate prediction of the PZ behavior. Kim and Engelhardt (1995, 2002) developed a model to capture the PZ deformations accurately. The resulting model performed well in comparison with the results of experimental data. However, from a practical point of view, it has complex parameters regarding material properties as well as deterioration laws. Also, it is hard to use the model in commercial structural analysis software.

Having known the concerns about the PZ behavior and its modeling techniques, researchers have been looking for more straightforward procedures to model PZ effects in the SMFs indirectly. Tsai and Popov (1990) examined two SMFs, 6- and 20-story, considering different conditions of the PZ. The building frames were designed per 1990 American Institute of Steel Construction Specification (AISC 1990) and 1998 Uniform Building Code requirements (UBC 1998). The PZs were designed for $0.8M_p$, where M_p is the flexural plastic strength of beam(s). The PZ behavior was explicitly modeled via the Scissors PZ model (see Fig. 2). Also, the PZ effect was implicitly modeled using different rigid-end-zone factors. In the former case, the rotational spring characteristics were adopted from previous (Krawinkler *et al.* 1975, FEMA 2000, Downs 2002, Charney and Downs 2004, Krawinkler and Mohasseb 1987, Popov 1987). In the latter case, two different rigid-end-zone factors were adopted; 0% and 50%. It was demonstrated that the roof drift results of the SMFs with PZ are relatively close to the results of the SMFs with 0% rigid-end zones. Also, the roof drift results of the SMFs with 50% rigid-end zones were approximately 27% less than those of the SMFs with PZ. Schneider and Amidi (1998) examined an 8-story SMF through non-linear static and dynamic analyses. Two conditions were considered; SMF with PZ and one centerline SMF model with rigid-
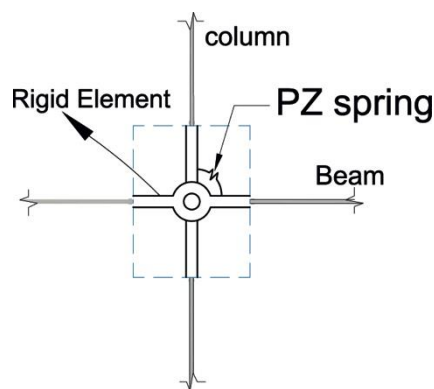
Fig. 2 Scissors PZ model

end-zone factor equals unity. It was shown that the drift responses for the centerline model with rigid-end zones are 25% smaller than those SMFs with PZ. Also, based on the results of pushover analysis, the stiffness of the SMFs with rigid-end zones is 30% greater than that of the SMF with PZ. Having seen the results of previous researches, Hamburger *et al.* (2009) recommended that a rational method should be adopted to model the PZ deformation in SMFs via a rigid-end-zone factor.

Recently, an Equivalent End Zone (EEZ) model was proposed to consider PZ deformations implicitly in the SMFs (Rafezy *et al.* 2014). The formulation of this model is based on the Scissors PZ model. However, researchers have mentioned some limitations and assumptions regarding this PZ model. Krawinkler *et al.* (1975) and FEMA (2000) stated that the PZ shear force and shear distortion have to be based on the difference between the beams' moments at the column face in the beam-to-column connection. Research showed that because the Scissors PZ model relates shear force and shear distortion of the PZ to the difference between the beams' moments at the beam-to-column intersection point, it leads to an approximate calculation of the shear force and shear distortion of the PZ. Another issue regarding the Scissors PZ model is its strength and stiffness characteristics (Downs 2002, Charney and Downs 2004). Downs (2002) and Charney and Downs (2004) stated that using the stiffness and strength characteristics of krawinkler's PZ model for the Scissors PZ model leads to inaccurate prediction of the deformations and stiffness of the PZ. Research also mentioned that there is not a clear relationship to define the stiffness of the Scissors PZ model.

Based on the discussions in the previous paragraphs, explicit modeling of the PZ in SMFs is of great importance. One way to contribute PZ effects into SMFs is to utilize Krawinkler's PZ model. However, the elements of the elements of the parallelogram of the Krawinkler's PZ model must be completely rigid, and due to computational problems, it cannot be applied in many software. As such, the PZ elements are modeled using elements with high axial, shear, and flexural rigidity. Given that utilizing these types of members raises issues regarding numerical convergence problems, the extent of the rigidity of these elements should be chosen carefully. Also, from a practical point of view,

Krawinkler's PZ model requires considering more degrees of freedom in the analytical model, and thus, the analysis will be time-consuming, especially in the case of dynamic time-history analysis. More importantly, practitioners prefer to adopt a more straightforward procedure than modeling PZ in the analytical model during the design procedure. Hence, it is worth finding an alternative method to avoid complexities regarding Krawinkler's PZ model and computational problems.

In this study, the authors try to simplify Krawinkler's PZ model and to propose an alternative approach to include PZ effect into SMFs. In this approach, the Krawinkler's PZ model is implicitly applied to SMFs using an Adjusted Rigid-End Zone (AREZ) model. The dimension of the AREZ will be calculated by an appropriate rigid-end-zone factor, β. The β depends on the properties of the connecting elements (i.e., beam(s) and columns) at each connection joint. In order to validate the proposed model, several interior and exterior connections are modeled utilizing the Open System for Earthquake Engineering Simulation software, OpenSees (Mckenna 1997). Furthermore, to demonstrate the applicability of the proposed model in SMFs, several SMFs ranging from 3- to 30-story, representing low- to high-rise buildings, are examined through linear static and dynamic time history analysis. In the analysis procedure, both Krawinkler's PZ model and AREZ are considered. Besides, two other extreme cases, β=0 and β=1, are considered to show the significance of PZ modeling in SMFs. The former represents a centerline SMF model, and the latter one is representative of a SMF with completely rigid-end zones. Also, non-linear dynamic analyses of three SMFs conducted to validate the degree of accuracy of the proposed model in the non-linear analysis of structures. Based on the analytical results, in addition to ease of implementation of the proposed model in the SMFs, the inter-story drift ratio (IDR) results of SMFs with the AREZ model show a good agreement with the IDR results of the same SMFs with Krawinkler's PZ model. The efficiency of the proposed model is evident in both linear and non-linear analysis of SMFs in this study. This simple model allows practitioners to consider PZ effects in the design procedure. Also, it can simply be applied to any structural frame analysis software.

2. Proposed model

The proposed model simplifies Krawinkler's PZ model (see Fig. 3(a)) through the AREZ, which is shown in Fig. 3(b). The dimensions of the AREZ are defined by an appropriate β factor, which is applied to the centerline model. In determining the β factor, the stiffness of the connection model with the AREZ is equalized to the stiffness of the connection with Krawinkler's PZ model.

In addition to the properties and geometries of a connection, the type of the connection (i.e., interior or exterior) plays an essential role in the response of PZ under lateral loads. Hence, in this study, the mentioned procedure in obtaining β is implemented for both interior and exterior connections, and Individual formulations are derived.

Several assumptions have been made during the formulation procedure. In the connection modeling, it is assumed that the moment at mid-span and mid-height of the story are zero. Also, it is assumed that the bay length and beam sections are equal in the left and right side of the connection. Furthermore, it is assumed that the story height and the column sections above and below the connection are the same. In the next subsections, for both interior and exterior connections, procedures to derive a relationship for β are presented in detail.

3. Interior connection

In order to obtain β for the interior connection type, two cases of the connections are considered; one connection with Krawinkler's PZ model, which is shown in Fig. 3(a), and one connection with the AREZ model (Fig. 3(b)). In the first model, there are rigid elements which form a parallelogram.

(a) Connection with Krawinkler's PZ model
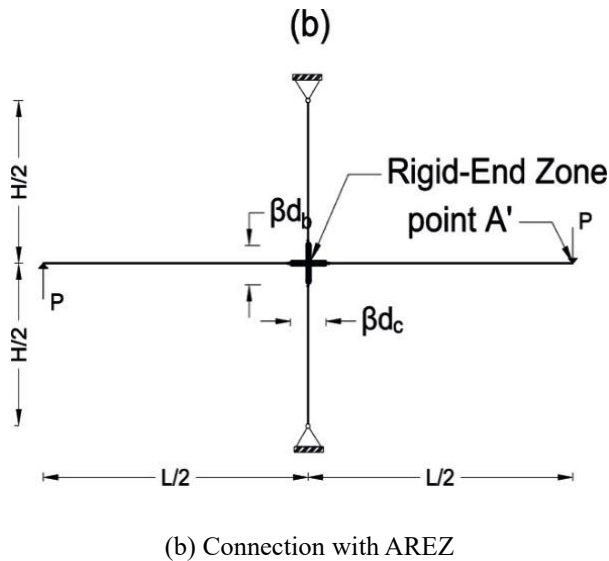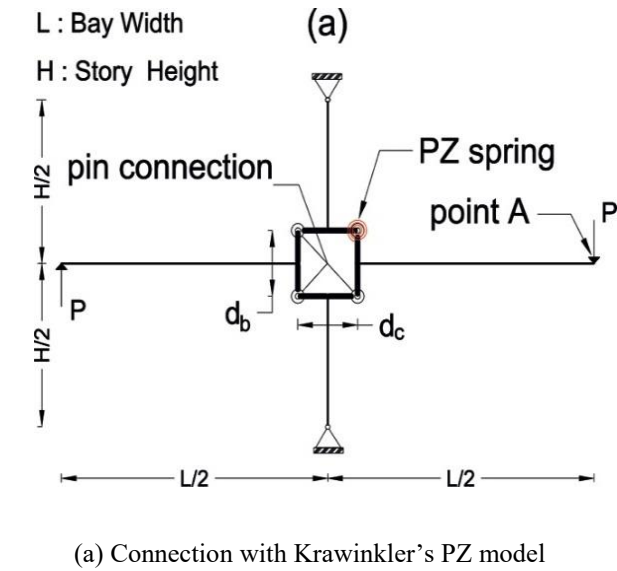

(b) Connection with AREZ

Fig. 3 Typical interior connection

Simple pin connections connect the corners of the parallelogram. A rotational spring, which represents the strength and stiffness behavior of the PZ, is attached to one of the four corners (i.e., the upper right corner). In the case of the AREZ model, the dimension of rigid-end-zones at the end of the members can be calculated by the β factor (Fig. 3(b)). The total deflection at the end of the beam, Δ_A, consists of the beam, column, and PZ deformations (see Fig. 4). For the case in which Krawinkler's PZ model is considered, Δ_A is as follows

$$\Delta_A = \delta_b + \delta_c + \delta_{pz} \tag{1}$$

Where δ_b, δ_c, δ_{pz} are the deflection components of the cantilever beam, the deflection component due to the rotation of the column (θ_c) at the connection joint, and the deflection component due to PZ distortion, respectively. δ_b can be calculated as follows

$$\delta_b = \frac{P\left(\frac{L - d_c}{2}\right)^3}{3EI_b} \tag{2}$$

In the above equation, d_c is the column depth, E is the modulus of elasticity, L is the beam span length (centerline dimension), I_b is the beam moment of inertia, and P is a concentrated force applied at the mid-span of the beam, respectively.

In order to calculate δ_c, first, a procedure to obtain θ_c is presented. Fig. 5 shows the columns above and below the connection joint. By using the conjugate beam method, θ_c is calculated as follows

$$\theta_c = \frac{PLH(1 - \psi)^3}{12EI_c} \tag{3}$$

In the Eq. (3), H is the column height, I_c is the column moment of inertia, and ψ is defined as the ratio of beam depth to the column height.

$$\psi = \frac{d_b}{H} \tag{4}$$

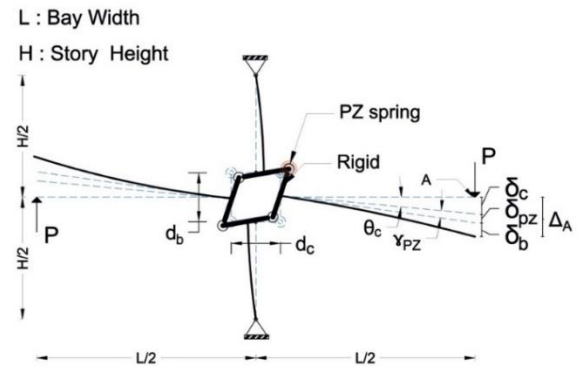Where d_b is the beam depth. Subsequently, δ_c can be calculated as follows

Fig. 4 The deformed shape of interior connection considering PZ

(a) The undeformed shape of the columns above and below the connection joint

(b) The deformed shape of the columns above and below the connection joint
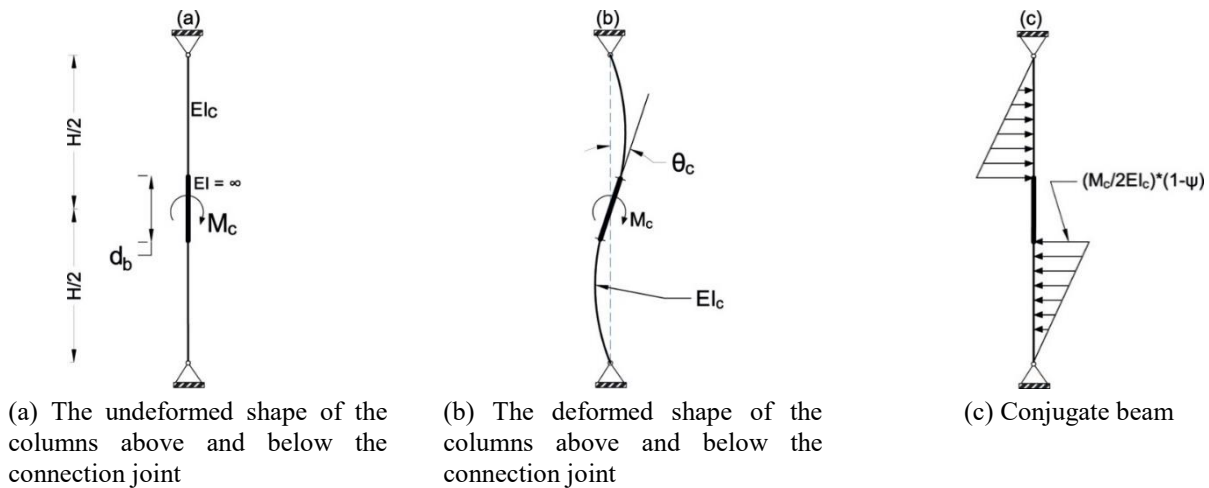
(c) Conjugate beam

Fig. 5 Columns above and below the connection joint
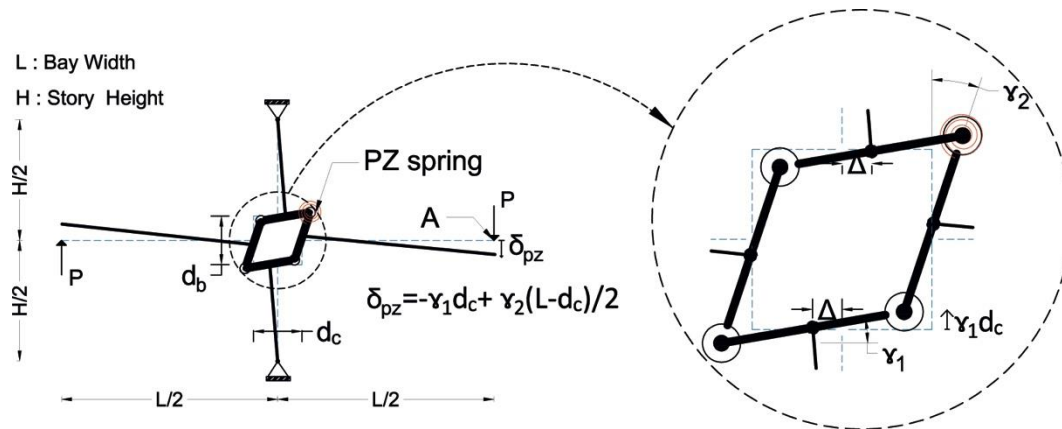

Fig. 6 The deformed shape of Krawinkler's PZ model

$$\delta_C = \frac{PL^2H(1-\psi)^3}{24EI_c} \tag{5}$$

Fig. 6 schematically shows the elements of PZ distortion, which is used to calculate δ_{pz}.

As shown in Fig. 6, δ_{pz} is written with respect to γ_1 and γ_2.

$$\delta_{pz} = -\gamma_1 d_c + \frac{\gamma_2(L - d_c)}{2} \tag{6}$$

In the above equation, γ_1 and γ_2 are distortion angles of the PZ with respect to horizontal and vertical axes, respectively. These parameters can be calculated by utilizing Eqs. (7) and (8), respectively. The mentioned equations are based on the deformed position of the PZ, which is shown in Fig. 6.

$$\gamma_1 = \frac{\Delta}{(H - d_b)/2} \tag{7}$$

$$\gamma_2 = \frac{2\Delta}{d_b} \tag{8}$$

In the above equations, Δ is the horizontal displacement of the column above or below the connection joint at the proximity of the PZ from corresponding original positions. The net PZ distortion, γ_{pz}, can be written as Eq. (9).

$$\gamma_{pz} = \gamma_1 + \gamma_2 = \frac{2\Delta H}{d_b(H - d_b)} \tag{9}$$

Therefore, γ_1 and γ_2 can be rewritten as follows

$$\gamma_1 = \psi \gamma_{pz} \tag{10}$$

$$\gamma_2 = (1 - \psi)\gamma_{pz} \tag{11}$$

In the following, γ_{pz} can be calculated by Eq. (12).

$$\gamma_{pz} = \frac{M_{pz}}{K_{pz}} \tag{12}$$

In Eq. (12), M_{pz} is the bending moment of the PZ, K_{pz} is the stiffness of the PZ (Kim and Engelhardt 1995, Kim and Engelhardt 2002). The mentioned variables are as follows
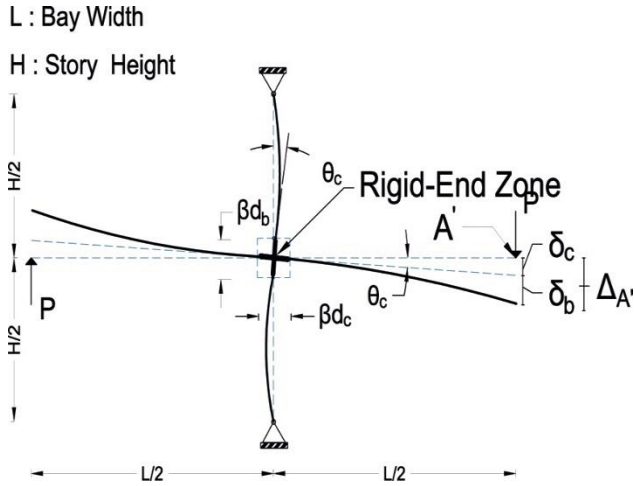
L : Bay Width

H : Story Height

Fig. 7 The deformed shape of interior connection with AREZ

$$M_{pz} = P(L - d_c) \qquad (13)$$

$$K_{pz} = \frac{G(d_c - t_{cf})t_p d_b}{(1 - \rho)} \qquad (14)$$

In Eq. (14), t_{cf} is the column flange thickness, t_p is the PZ thickness (column web thickness plus doublar plate thickness), G is the elastic shear modulus, and ρ is defined as below (Kim and Engelhardt 1995, Kim and Engelhardt 2002)

$$\rho = \frac{d_b - t_{bf}}{H} \qquad (15)$$

In the above equation, Eq. (15), t_{bf} is the thickness of the beam flange. Substituting Eqs. (10)-(14) into Eq. (6), δ_{pz} can be rewritten as follows

$$\delta_{pz} = \frac{P(L - d_c)(1 - \rho)}{2G(d_c - t_{cf})t_p d_b}[L(1 - \psi) - d_c(1 + \psi)] \qquad (16)$$

In a connection joint with the AREZ, Fig. 7, the total deflection at the end of the beam is as follows

$$\Delta_{A'} = \delta_{b'} + \delta_{c'} \qquad (17)$$

Where $\Delta_{A'}$, $\delta_{b'}$, $\delta_{c'}$ are total deflection at the end of the beam, the deflection component of the cantilever beam, the deflection component due to the rotation of the column at the connection joint, respectively. The procedures are the same as those in the case of the connection with Krawinkler's PZ. $\delta_{b'}$ and $\delta_{c'}$ are written as below.

$$\delta_{b'} = \frac{P\left(\frac{L - \beta d_c}{2}\right)^3}{3EI_b} \qquad (18)$$

$$\delta_{c'} = \frac{PL^2 H(1 - \beta\psi)^3}{24EI_c} \qquad (19)$$

Equating the end beam deflections of two connection models, connection with Krawinkler's PZ model and the one with the AREZ, leads to a cubic equation, Eq. (20),

with respect to β. Solving the Eq. (20) leads to a β factor, which can be applied as the rigid-end-zone factor in a centerline model. This β is specific to each connection joint and is based on the specification of connecting elements.

$$-a_1\beta^3 + a_2\beta^2 - a_3\beta + a_4 = 0 \qquad (20)$$

In the Eq. (20), a_1, a_2, a_3, a_4, are coefficients of the cubic equation. These coefficients depend on the beam(s) and columns specifications in the connection joint, the length of the beam span, and the height of the column. The coefficients are as follows

$$a_1 = \frac{d_c^3(1 + \xi\ v^2\mu^3)}{24EI_b} \qquad (21)$$

$$a_2 = \frac{d_c^2 L(1 + \xi\ v\ \mu^2)}{8EI_b} \qquad (22)$$

$$a_3 = \frac{d_c L^2(1 + \xi\ \mu)}{8EI_b} \qquad (23)$$

$$a_4 = a_1 - a_2 + a_3 \ldots$$
$$-\frac{[L(1 - \psi) - d_c][L(1 - \psi) - d_c(1 + \psi)](1 - \rho)}{2G(d_c - t_{cf})t_p d_b} \qquad (24)$$

Where

$$\xi = \frac{I_b}{I_c} \qquad (25)$$

$$\mu = \frac{d_b}{d_c} \qquad (26)$$

$$v = \frac{L}{H} \qquad (27)$$

4. Exterior connection

Figs. 8(a) and 8(b) show exterior connections with both Krawinkler's PZ and AREZ schematically. The deflection components of the exterior connections are shown in Figs. 9-10. The procedures for calculating the deflection components for the exterior connection are the same as those of the interior connection. To calculate the β factor for the exterior connection, an equation similar to that of the interior connection, Eq. (20), is obtained except that the coefficients of the Eq. (20) for the exterior connection differ from the interior connection. The coefficients of the Eq. (20) for the exterior connection are presented through Eqs. (28)-(31).

$$a_1 = \frac{d_c^3(2 + \xi\ v^2\mu^3)}{48EI_b} \qquad (28)$$

$$a_2 = \frac{d_c^2 L(2 + \xi\ v\ \mu^2)}{16EI_b} \qquad (29)$$

$$a_3 = \frac{d_c L^2(2 + \xi\ \mu)}{16EI_b} \qquad (30)$$

$$a_4 = a_1 - a_2 + a_3 \ldots$$
$$-\frac{[L(1 - \psi) - d_c][L(1 - \psi) - d_c(1 + \psi)](1 - \rho)}{4G(d_c - t_{cf})t_p d_b} \qquad (31)$$
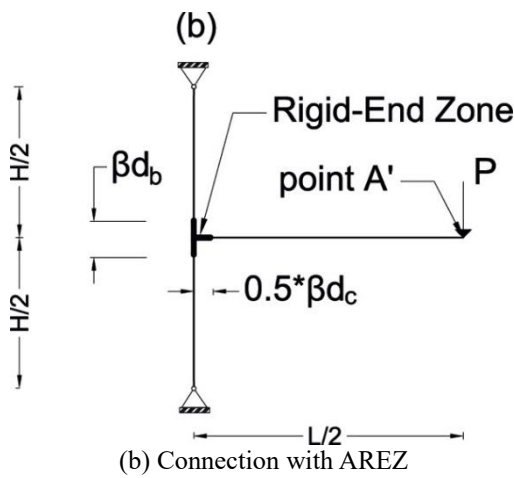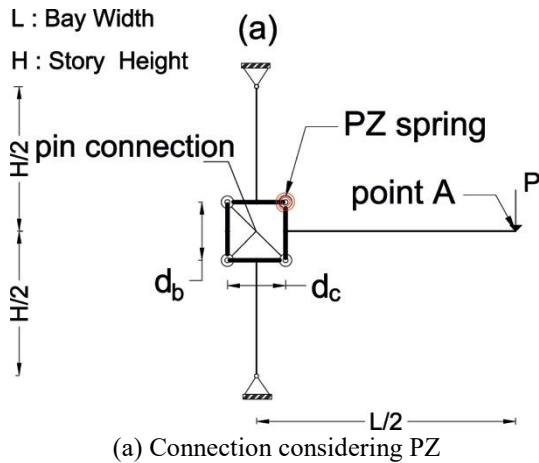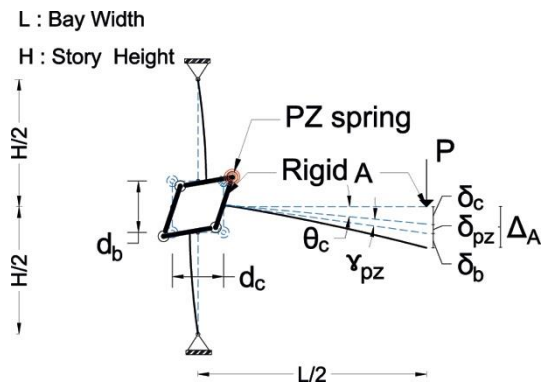
(a) Connection considering PZ

(b) Connection with AREZ

Fig. 8 Typical exterior connection

Fig. 9 The deformed shape of the exterior connection considering PZ

Fig. 10 The deformed shape of the exterior connection with AREZ

(a) Connection with krawinkler's PZ model

(b) Connection with AREZ model

Fig. 11 The modeling details of an interior connection in the OpenSees software

5. Validation procedure

In order to show the efficiency of the proposed model, a validation procedure is conducted. Several interior and exterior connections have been taken apart from well-known SMFs. These connections and their specifications are summarized in Table 1.
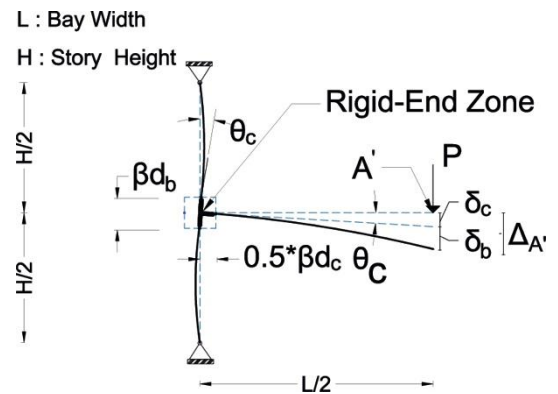
Table 1 Proposed model validation results

Building	Conn. No	Beam section	Column Section	Conn. Type	Bay Width (m)	Story Height (m)	Beam end deflection	
							Connection with AREZ model $\Delta_{A'}$(m)	Connection with Krawinkler's PZ model Δ_A(m)
SAC 3 Loss Angeles (Gupta and Krawinkler 1999)	1	W33x118	W14x311	Interior	9.14	3.96	0.41903	0.4203
	2	W24x68	W14x311	Interior	9.14	3.96	0.1064	0.1065
	3	W30x116	W14x257	Exterior	9.14	3.96	0.4208	0.4232
	4	W24x68	W14x257	Exterior	9.14	3.96	0.9709	0.9747
SAC 9 Loss Angeles (Gupta and Krawinkler 1999)	5	W36x135	W14x455	Interior	9.14	3.96	0.2409	0.2417
	6	W36x135	W14x370	Interior	9.14	3.96	0.3094	0.3104
	8	W36x160	W14x370	Exterior	9.14	3.96	0.2098	0.2114
	10	W27X84	W14X233	Exterior	9.14	3.96	0.6790	0.6822
SAC20 Loss Angeles (Gupta and Krawinkler 1999)	11	W30x99	W24x335	Interior	6.10	3.96	0.1254	0.1262
	12	W30x108	W24x229	Interior	6.10	3.96	0.1373	0.1384
	13	W30x99	W24x192	Interior	6.10	3.96	0.1600	0.1613
	14	W30x99	W24x131	Interior	6.10	3.96	0.1634	0.1642
SAC 3 Seattle (Gupta and Krawinkler 1999)	17	W24x76	W14x176	Interior	9.14	3.96	0.1139	0.1141
	18	W24X84	W14x176	Interior	9.14	3.96	0.1006	0.1008
	19	W24X76	W14x176	Exterior	9.14	3.96	0.9587	0.9625
SAC 9 Seattle (Gupta and Krawinkler 1999)	20	W30x116	W24x229	Interior	9.14	3.96	0.3950	0.3963
	21	W24x76	W24x207	Interior	9.14	3.96	0.8265	0.8282
	22	W24x76	W24x162	Interior	9.14	3.96	0.8735	0.8754
	23	W30x116	W24x229	Exterior	9.14	3.96	0.3443	0.3467
	24	W24x76	W24x207	Exterior	9.14	3.96	0.7539	0.7575
	25	W24x76	W24x162	Exterior	9.14	3.96	0.7871	0.7909
SAC 20 Seattle (Gupta and Krawinkler 1999)	26	W30x132	W24x229	Interior	6.10	3.96	0.1110	0.1119
	27	W30x132	W24x192	Interior	6.10	3.96	0.1207	0.1217
	28	W27x94	W24x162	Interior	6.10	3.96	0.3464	0.3481
	29	W30x132	W24x229	Exterior	6.10	3.96	0.0900	0.0919
	30	W30x132	W24x192	Exterior	6.10	3.96	0.0963	0.0984
	31	W27x94	W24x192	Exterior	6.10	3.96	0.1503	0.1530
	32	W24x62	W24x162	Exterior	6.10	3.96	0.2902	0.2942
6 Story (Kalkan and Kunnath 2006, Kalkan and Chopra 2010)	33	W27x102	W14x176	Interior	6.10	3.96	0.2926	0.2983
	34	W24x68	W14x132	Interior	6.10	3.96	0.4900	0.5192
	36	W24x68	W14x132	Exterior	6.10	3.96	0.3726	0.3765
	37	W24x84	W14x90	Exterior	6.10	3.96	0.3769	0.3980
13 Story (Kalkan and Kunnath 2006, Kalkan and Chopra 2010)	38	W33x152	W14x426	Interior	9.75	3.96	0.3465	0.3475
	39	W33x152	W14x398	Interior	9.75	3.96	0.3587	0.3598
	40	W33x152	W14x426	Exterior	9.75	3.96	0.2822	0.2839
	41	W33x152	W14x398	Exterior	9.75	3.96	28.871	0.2905

Then, these connections are modeled in the OpenSees software (Mckenna 1997) in two manners; connections with krawinkler's PZ model, and connections with the AREZ model. In the former case, beam and column elements are modeled using the elasticBeamColumn element of the OpenSees library. The PZ is modeled utilizing eight rigid elements (elasticBeamColumn with high axial, shear, and flexural rigidity), which are connected through twelve

nodes to form a parallelogram (see Fig. 11(a) and 11(b)).

Four corners of the parallelogram are connected as simple pin connections. In order to model the stiffness of the PZ in the connection joint, a rotational spring is placed at one corner of the parallelogram (e.g., the upper right corner). This spring has a linear behavior and affects the elastic stiffness of the connection joint, and consequently, beam tip deflection or story drift. In the connection joint with the AREZ, the effect of krawinkler's PZ model is applied to the connection area through rigid-end zones of the connecting beam(s) and columns. The rigid-end zones at the end of each connecting element (i.e., beam(s) and columns) are modeled using rigid elements as defined before for the krawinkler's model. The dimensions of the rigid-end zones are determined by multiplying β, which is obtained from Eq. (20), to the depth of the beam(s) and columns of the connection joint. Table 1 shows the comparison between the analysis results of the connections with both Krawinkler's PZ and AREZ models.

6. Structural frame models

In order to show the efficiency of the proposed model, a series of six SMFs ranging from 3- to 30-story is selected. Three of the building frame models are as part of the SAC steel project; 3- and 9-story of Lose Angeles structures, SAC 3 and SAC 9, and 20-story of Seattle structures, SAC 20 (Gupta and Krawinkler 1999). Two other building frame models are 6- and 13-story SMFs, which have been used as case studies in several researches (Kalkan and Kunnath 2006a, Kalkan and Kunnath 2006b, Kalkan and Chopra 2010). The last building frame model is a 30-story SMF (Poursha *et al.* 2010). The information, including section properties, dimensions, and seismic mass of model buildings, are provided in the appendix.

SAC 3 is a three-story and four-bay perimeter SMF, which is an office building, that was designed for the city of Loss Angeles, California. The bay width and story heights are 9.15m and 3.96m, respectively. The design yield strengths of beams and columns are 248×10⁶ Pa and 345×10⁶ Pa, respectively. The structure was designed based on the seismic design requirements of the 1994 Uniform Building Code (UBC 94). At one bay, the first one from the right, all the beam connections are simple pin connection. Detailed information is provided in (Gupta and Krawinkler 1999).

SAC 9 is a nine-story and five-bay perimeter SMF, which is an office building. The building was designed for the city of Loss Angeles, California. The building has one basement, and its bay width and the height of typical stories are 9.15 m and 3.65 m, respectively. The height of the basement is 5.49 m. The design yield strengths of beams and columns are 248×10⁶ Pa and 345×10⁶ Pa, respectively. The structure was designed based on UBC 94. At one bay, the exterior one on the right-hand side, all the right beam connections are simple pin connection. At the ground level, the building is restrained in a horizontal direction. Detailed information is provided in (Gupta and Krawinkler 1999).

SAC 20 is a twenty-story and five-bay perimeter SMF, which is used as an office building. The building was designed for the city of Seattle, Washington. The building has two basements. The bay width and the height of typical stories are 6.1 m and 3.96 m, respectively. The height of the basements is 3.65 m, and the height of the first story is 5.49m. The design yield strength of beams and columns is 345×10⁶ Pa. The structure was designed based on UBC 94. At the ground level and also at the level of basement 1, the building is restrained in the horizontal direction. Detailed information is provided in (Gupta and Krawinkler 1999).

The 6-story SMF building is an instrumented building which is located in Burbank, California. The building has a rectangular plan, and its dimensions are 36.6 m by 36.6 m. The bay width is 6.1 m. The height of the first story and typical stories are 5.3 m and 4.0 m, respectively. The design yield strength of beams and columns is 303×10⁶ Pa, as established by coupon tests (Anderson and Bertero 1997). The structure was designed based on seismic design requirements of the 1973 Uniform Building Code (UBC 73). At one bay, the first one from the right, all the right beam connections are simple pine connection. Detailed information is provided in (Kalkan and Kunnath 2006a, Kalkan and Kunnath 2006b).

The 13-story SMF building is an instrumented building which is located in South San Fernando Valley, California, about 5 km southwest of the Northridge epicenter. The N-S direction frame was adopted. The building has a rectangular plan, and its dimensions are 53.3 m and 53.3 m. The building has one basement. The bay width, the height of the basement, and the height of the first story are 9.75 m, 4.42 m, and 4.88 m, respectively. The height of typical stories is 4.013 m. The design yield strength of beams and columns is 303×10⁶ Pa, as established by coupon tests (Anderson and Bertero 1997). The structure was designed based on UBC 73. At the ground level, the building is restrained in a horizontal direction. Detailed information is provided in (Kalkan and Kunnath 2006a, Kalkan and Kunnath 2006b, Kalkan and Chopra 2010).

The 30-story SMF building is a thirty-story and three-bay perimeter steel moment frame as an office building. The building was designed for the city of Tehran, Iran. The bay width and the height of all stories are 5.0 m and 3.2 m, respectively. The design yield strength of beams and columns is 230×10⁶ Pa. The structure was designed based on the Iranian code of practice for the seismic resistant design of buildings (2800 standard 2005). The seismicity of the location is the highest based on the 2800 standard. Detailed information is provided in (Poursha *et al.* 2010).

All SMFs are modeled in the OpenSees platform (Mckenna 1997). All Beam and column members are modeled as linear elastic elements (elasticBeamColumn elements). The PZ spring was modeled by a linear-elastic material, and the stiffness of the spring is given by Eq. (14). In order to include the second-order effects, *P-Δ*, leaning columns are modeled, and the gravity load tributary to the half of the building is applied to the leaning columns at the level of stories. Structural frame models are examined with the various condition of the PZs. First, the SMF models

Table 2 Characteristics of building models

No. Stories	h (m)	R_u	Period of vibrational modes (sec)								
			$T_1^{(1)}$	$T_1^{(2)}$	$T_1^{(3)}$	$T_2^{(1)}$	$T_2^{(2)}$	$T_2^{(3)}$	$T_3^{(1)}$	$T_3^{(2)}$	$T_3^{(3)}$
3	11.88	12	1.01	0.9797	0.9798	0.3271	0.2978	0.3159	0.1714	0.1360	0.1602
6	25.30	12	1.40	1.44	1.43	0.51	0.52	0.52	0.31	0.29	0.30
9	40.84	12	2.2529	2.2119	2.1918	0.8374	0.8155	0.8264	0.4876	0.4771	0.66
13	57.50	12	3.08	2.9773	3.0014	1.10	1.0458	1.0617	0.66	0.6185	0.6361
20	88.08	12	3.7619	3.5813	3.5201	1.3587	1.2873	1.2725	0.7927	0.7487	0.7418
30	96.0	8	3.8605	3.5271	3.5393	1.3911	1.2757	1.2773	0.8040	0.7397	0.7409

h: Building height

R_u: Response modification factor

(1): Centerline model; (2): Model with PZ (Krawinkler's PZ model); (3): Model with AREZ

with Krawinkler's PZ model. Second, the frame models with the AREZ. The third and fourth cases consider two extreme conditions; $\beta=0$ represents the centerline model, and $\beta=1$ is a representative of completely rigid PZ. For the non-linear cases, non-linear models of 3-, 9-, and 20-story SMFs are developed in the OpenSees platform (Mckenna 1997). Model buildings are idealized based on the concentrated plasticity approach. Rotational springs, located at the plastic hinge regions, are used to model the non-linear behavior of the beams and PZs. Columns were assumed to remain elastic except the column bases, which are assigned the non-linear rotational springs to simulate the expected behavior of SMFs at the base connections.

The bilin material was assigned to rotational springs of beam elements to simulate the modified Ibarra-Medina-Krawinkler deterioration model with a bilinear hysteretic response. The hysteretic response of this material had been calibrated with respect to experimental data, and regression formulas have been provided to estimate the deterioration parameters of the model. These relationships were developed by Lignos and Krawinkler (2009, 2011). The non-linear behavior of the PZ was simulated using the three-linear relationship developed by Krawinkler *et al.* (1971). Characteristics of Krawinkler's PZ model can be found in Gupta and Krawinkler (1999). For each SMF model, four types of numerical models are employed. The first one represents the SMF with krawinkler's PZ model. the second one considers the centerline SMF model with AREZ. the third and fourth models are SMFs with two extreme PZ conditions, $\beta=0$ and $\beta=1$. Table 2 summarizes the building models' characteristics.

7. Analysis procedure

Linear static and dynamic time-history analyses are conducted to demonstrate the efficiency of the proposed model. Furthermore, non-linear dynamic analyses were conducted to validate the proposed model, AREZ, in the non-linear analysis of SMFs.

Table 3 Equivalent static lateral force method information for frame building under investigation

No. Stories	h(m)[1]	Rw[2]	T(sec)[3]	W(N)[4]	V(N)[5]
3	11.88	12	0.546	14676996.13	1098732.08
6	25.3	12	0.962	13733403.78	704555.60
9	40.84	12	1.378	49790189.87	2008745.70
13	57.5	12	1.781	77026828.65	2621034.51
20	88.08	12	2.452	55130902.65	1515726.17
30	96	8	2.616	16560195.23	654137.67

1: Height of building; 2: Response modification factor; 3: Code-based period; 4: Total seismic weight; 5: Static base shear

7.1 Static analysis

For the linear analysis of building models, the Equivalent Lateral Force (ELF) method is used in the static lateral load analysis. Given that this paper just compares the frame models with krawinkler's PZ model and the AREZ, for the sake of simplicity, the base shear and distribution of lateral forces over the height of the buildings are per UBC 94 for all building models. Table 3 shows the base shear values as well as the weights of building frame models under consideration.

7.2 Dynamic analysis

In the case of linear and non-linear dynamic time-history analysis, an ensemble of 20 scaled ground motion records is used. The ground motion records were provided for the Loss Angeles area (la records) as part of the SAC steel research project. These records have a return period of 475 years. All ground motion records belong to the stiff soil condition. Table 4 shows ground motion characteristics. It should be noted that in this study, the authors just used the scaled record and did not conduct any further scaling procedures. As mentioned in the static analysis section, the goal is the comparison of the story drift ratios of SMFs with

Table 4 Ground motion characteristics

Record Name	Earthquake Name	Earthquake Magnitude	Distance (km)	Scale Factor	Number of Points	DT (sec)	Duration (sec)	PGA (g)
LA01	Imperial Valley, 1940, El Centro	6.9	10	2.01	2674	0.02	39.38	0.461
LA02	Imperial Valley, 1940, El Centro	6.9	10	2.01	2674	0.02	39.38	0.676
LA03	Imperial Valley, 1979, Array #05	6.5	4.1	1.01	3939	0.01	39.38	0.394
LA04	Imperial Valley, 1979, Array #05	6.5	4.1	1.01	3939	0.01	39.38	0.488
LA05	Imperial Valley, 1979, Array #06	6.5	1.2	0.84	3909	0.01	39.08	0.302
LA06	Imperial Valley, 1979, Array #06	6.5	1.2	0.84	3909	0. 01	39.08	0.235
LA07	Landers, 1992, Barstow	7.3	36	3.2	4000	0.02	79.98	0.421
LA08	Landers, 1992, Barstow	7.3	36	3.2	4000	0.02	79.98	0.426
LA09	Landers, 1992, Yermo	7.3	25	2.17	4000	0.02	79.98	0.520
LA10	Landers, 1992, Yermo	7.3	25	2.17	4000	0.02	79.98	0.360
LA11	Loma Prieta, 1989, Gilroy	7	12	1.79	2000	0.02	39.98	0.665
LA12	Loma Prieta, 1989, Gilroy	7	12	1.79	2000	0.02	39.98	0.970
LA13	Northridge, 1994, Newhall	6.7	6.7	1.03	3000	0.02	59.98	0.678
LA14	Northridge, 1994, Newhall	6.7	6.7	1.03	3000	0.02	59.98	0.657
LA15	Northridge, 1994, Rinaldi	6.7	7.5	0.79	2990	0.005	14.945	0.534
LA16	Northridge, 1994, Rinaldi	6.7	7.5	0.79	2990	0.005	14.945	0.580
LA17	Northridge, 1994, Sylmar	6.7	6.4	0.99	3000	0.02	59.98	0.569
LA18	Northridge, 1994, Sylmar	6.7	6.4	0.99	3000	0.02	59.98	0.817
LA19	North Palm Springs, 1986	6	6.7	2.97	3000	0.02	59.98	1.019
LA20	North Palm Springs, 1986	6	6.7	2.97	3000	0.02	59.98	0.987

Table 5 Median base shear values from time history analysis for individual buildings

Buildings	3-Story		6-Story		9-Story		13-Story		20-Story		30-Story	
	a	b	a	b	a	b	a	b	a	b	a	b
V (N)	1574314.6	1539440.5	1028286.5	998394.4	2757043.3	2700248.4	2645446.3	2501964.5	1593246.2	1588264.2	848934.2	836977.3

a) Frames with Krawinkler's PZ; b) Frames with AREZ

krawinkler's PZ model and those of SMFs with the AREZ model. More details about the selection and scaling procedure of the ground motion records are provided in (Somerville 1997). Table 5 shows the median base shear forces for individual buildings for this ground motion ensemble.

8. Numerical results

In this section, the IDR results from linear static and dynamic time history analysis of steel moment frames are presented (Figs. 12-23). In the dynamic time history analysis, the median IDR results of SMFs for ground motion ensemble are considered here. Besides, Figs. 24-26 show the IDR results for 3-, 9-, and 20-story SMFs under non-linear time-history analysis. The median IDR results of
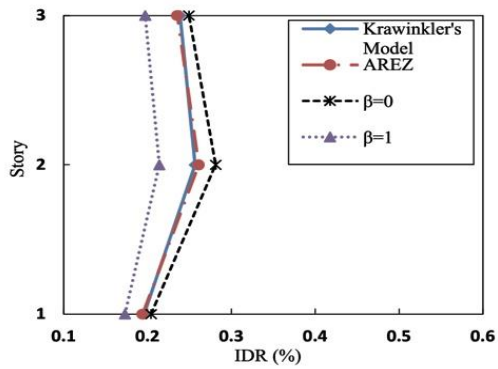
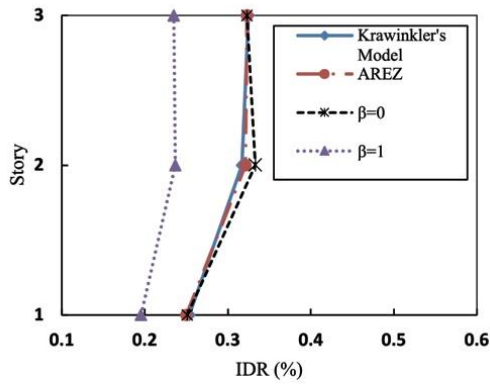Fig. 12 The 3-story IDRs for ELF method

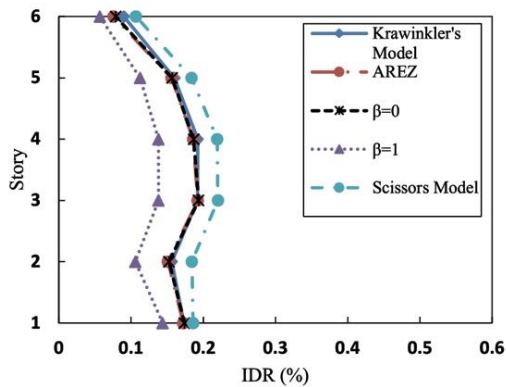Fig. 13 The 3-story median IDRs under earthquake excitation

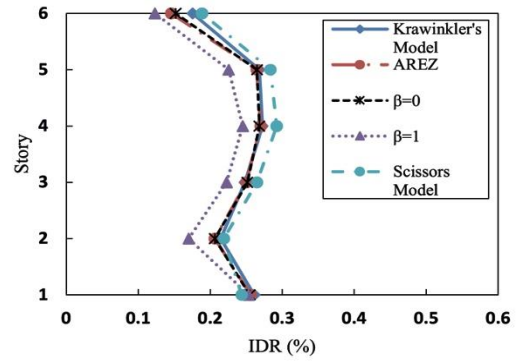Fig. 14 The 6-story IDRs for ELF method

Fig. 15 The 6-story median IDRs under earthquake excitation
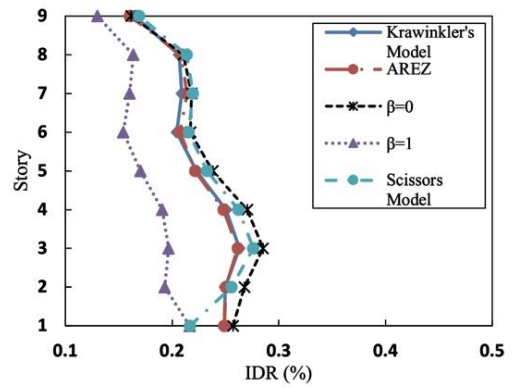

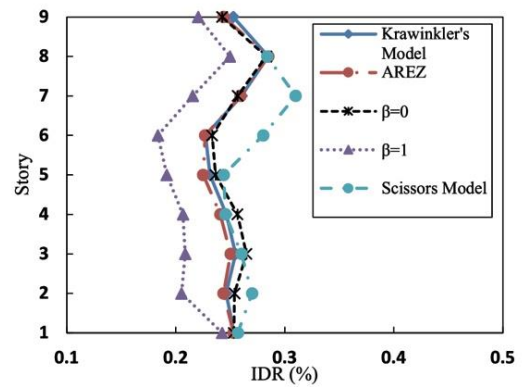Fig. 16 The 9-story IDRs for ELF method

Fig. 17 The 9-story median IDRs under earthquake excitation

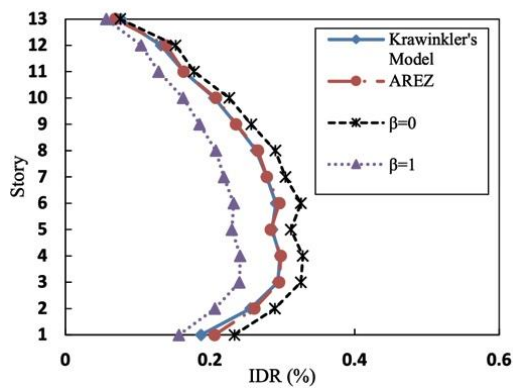building models are provided to compare the results for different PZ conditions.
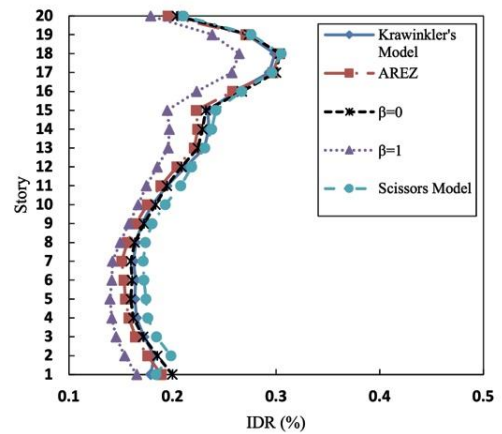
Fig. 18 The 13-story IDRs for ELS method

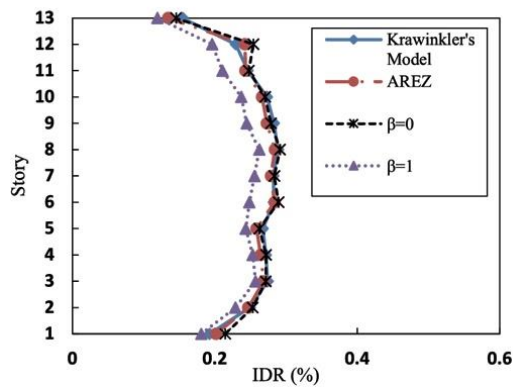Fig. 19 The 13-story median IDRs under earthquake excitation

Fig. 20 The 20-story IDRs for ELF method

Fig. 21 The 20-story median IDRs under earthquake excitation
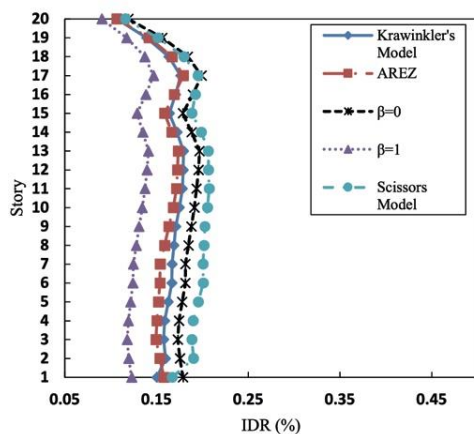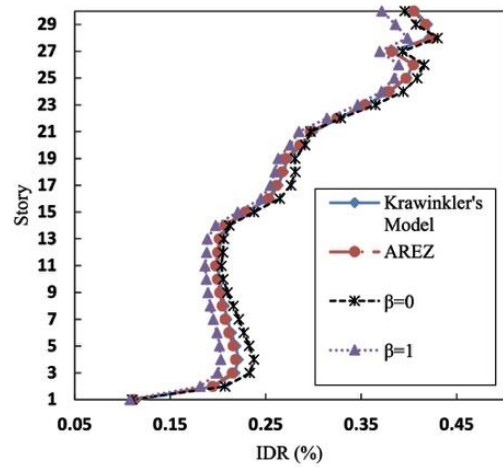

Fig. 22 The 30-story IDRs for ELF method

Fig. 23 The 30-story median IDRs under earthquake excitation

9. Discussion of the numerical results

As shown in Figs. 12-23, there is a good agreement between the IDR results of SMFs with Krawinkler's PZ model and those of SMFs with the AREZ model under static and dynamic analyses. These figures clearly show the efficiency of the proposed model, as it reasonably calculates the deformation of Krawinkler's PZ model, and subsequently, the IDRs of SMFs under consideration. As can be seen in Figs. 12-23, while the number of stories in the SMFs increases, the effect of PZ deformations becomes smaller, specifically in the case of dynamic analysis. Also, these figures show that the impact of PZ modeling in SMFs is more pronounced in the case of static analysis than dynamic analysis. Another observation from the IDR results of static and dynamic analysis of SMFs is that neither $\beta=0$ nor $\beta=1$ is reliable factors to consider PZ deformations. Although the centerline model assumption may sometimes predict IDR response of SMFs accurately, there is not a specific situation to rely upon centerline model assumption as an alternative to PZ modeling in SMFs. In order to demonstrate the efficiency of Krawinkler's model and the AREZ model compared to the Scissors PZ model, the 6-, 9-, and 20-story SMFs under consideration are also modeled considering the Scissors PZ model. These building frames are selected since they have relatively weak PZ to show the superiority of the krawinkler's PZ model, and subsequently, the AREZ model over the Scissors PZ model. The stiffness relationship of the Scissors PZ model is the same as the relationship in (Rafezy *et al.* 2014). These SMFs are analyzed through static and dynamic time-history analyses. The results from both the static and dynamic analyses show the superiority of the krawinkler's PZ model, as well as the AREZ model, over the Scissors PZ model. Figs. 14-17 and 20-21 show the comparison of the IDR results of building frame models with different PZ conditions; Krawinkler's PZ model, SMFs with the AREZ model, centerline model, SMFs with completely rigid-end zones, and Scissors PZ models. As these figures show, for SMFs with relatively weak PZs, the centerline model (i.e., $\beta= 0$) predicts IDRs better than SMFs with the Scissors PZ model; however, none of them has the accuracy of Krawinkler's model. These figures also show the IDR results of the SMFs with two extreme PZ conditions; $\beta= 0$ and $\beta=1$. These two extreme conditions are considered to emphasize the accuracy of the Krawinkler's PZ model, and as such, the accuracy and efficiency of the AREZ model in comparison with the Scissors PZ model.

When it comes to the non-linear analysis of SMFs, Figs. 24-26 show the applicability of the proposed model, even in the non-linear analysis of SMFs. These figures clearly show how accurately the AREZ model can predict the Krawinkler's PZ deformations in SMFs. In the authors' opinion, this is due to the increased length of the Beams and columns in SMFs with AREZ, such that this increase in the length of beams and columns reduces their stiffness, and to some extent, compensate the non-linear behavior of the PZ. Above all, based on the analysis results, in addition to the simplicity of the proposed model and its accuracy in the
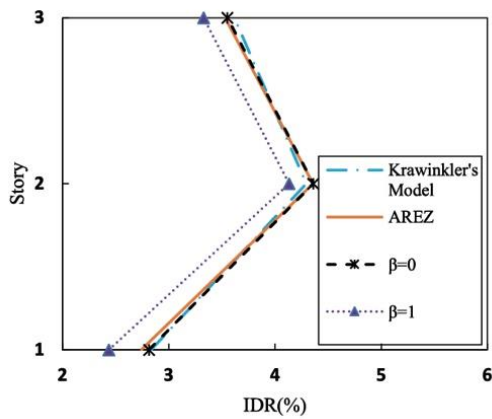

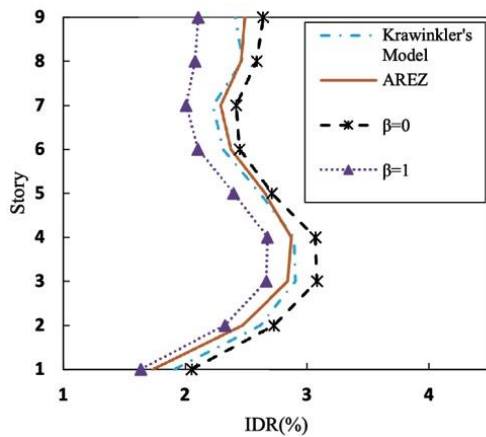Fig. 24 The 3-story median IDRs for non-linear time-history analysis

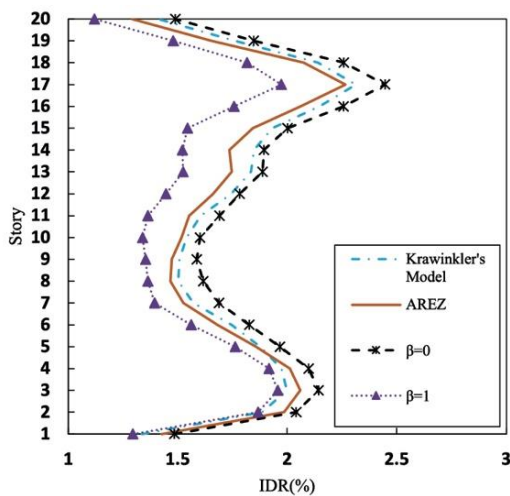Fig. 25 The 9-story median IDRs for non-linear time-history analysis

Fig. 26 The 20-story median IDRs for non-linear time-history analysis

linear analysis of SMFs, this model is capable of predicting the non-linear behavior of SMFs with acceptable accuracy.

10. Conclusions

In Krawinkler's PZ model, it is assumed that the elements of the parallelogram are rigid; however, they cannot be modeled completely rigid. Instead, they are modeled using elements with high axial, shear, and flexural rigidity. Given the fact that utilizing these types of elements causes some issues regarding numerical convergence problems, the amount of rigidity of these elements should be chosen carefully. Besides, from a practical point of view, Krawinkler's PZ model requires considering more degrees of freedom in the analytical model. Subsequently, the modeling and analysis will be time-consuming, especially in the case of dynamic time-history analysis. More importantly, practitioners prefer to adopt a more straightforward procedure to consider PZ deformation in the analytical model during the design procedure instead of some complex concepts related to PZ calibration parameters. Hence, in this study, an attempt is made to find a practical and straightforward approach to consider Krawinkler's PZ deformation effect in SMFs. The proposed model will help to overcome the uncertainties and complexities regarding Krawinkler's PZ model. In the proposed model, AREZ, the PZ effect is modeled implicitly through an appropriate rigid end-zone factor, which is applied to the centerline model. Also, it is feasible to apply to any structural analysis software. The AREZ model is compatible with both exterior and interior connections. It is believed that the AREZ model accurately takes into account the PZ deformations of Krawinkler's model. In order to show the efficiency of the proposed model, a validation procedure is conducted in two steps. In the first step, the proposed model is applied to 41 connection specimens, which have been taken apart from well-known building models. In the second step, linear static and dynamic time-history analyses are performed on the building models ranging from 3- to 30-story. Further non-linear time-history analyses have shown the validity of the proposed model in the non-linear analysis of SMFs. In these building models, four conditions of the PZ are considered; Krawinkler's PZ model, the AREZ model, the centerline model, $\beta=0$, and a model with a completely rigid-end zone, $\beta=1$. Both validation steps showed an acceptable accuracy of the proposed model.

Following conclusions can be drawn from this study:
- The proposed model avoids complexities regarding modeling procedure as well as complex concepts related to behavioral parameters of the Krawinkler's PZ model.
- When non-linear analysis of SMFs was adopted, the AREZ model showed that it has a reasonable accuracy on predicting the IDR demands of SMFs.
- The proposed model has superiority over the EEZ model and the Scissors PZ model.
- This simple model, AREZ, allows practitioners to consider PZ effects in the design procedure simply,

and also it can simply be applied to any structural frame analysis software.
- The proposed model, AREZ, reasonably predicts deformations related to Krawinkler's PZ model in SMFs both in the static and dynamic time-history analysis.
- The centerline model, $\beta=0$, and a completely rigid-end zone, $\beta=1$, are not reliable models for considering PZ behavior in SMFs.

References

AISC (1990), Load and resistance factor design specification for structural steel buildings, American Institute of Steel Construction; Chicago, USA.

Anderson, J.C. and Bertero, V.V. (1997), "Implications of the landers and big bear earthquakes on earthquake resistant design of structures", UCB/EERC-97/08; Earthquake Engineering Research Center, University of California, Berkeley, USA.

Adan, S.M. and Reaveley, R.D. (2006), "RBS moment connections without continuity plates", *Proceedings of the 8th U.S. National Conference on Earthquake Engineering*, San Francisco, USA, April.

Bertero, V.V., Krawinkler, H. and Popov, E.P. (1973), "Further studies on seismic behavior of steel beam-to-column subassemblages", UBC/EERC-73/27; Earthquake Engineering Research Center, University of California, Berkeley, USA.

Bayat, M. and Zahrai, S.M. (2017), "Seismic performance of mid-rise steel frames with semi-rigid connections having different moment capacity", *Steel Compos. Struct.*, **25**(1), 1-17. https://doi.org/10.12989/scs.2017.25.1.001.

Charney, F.A. and Downs, W.M. (2004), "Modeling procedures for panel zone deformations in moment resisting frames", *Proceedings of National Conference on Connections in Steel Structures V: Innovative Steel Connections*, Amsterdam, the Netherlands, June.

Castro, J.M., Elghazouli, A.Y. and Izzuddin, B.A. (2005), "Modelling of the panel zone in steel and composite moment frames", *Eng. Struct.*, **27**(1), 129-144. https://doi.org/10.1016/j.engstruct.2004.09.008.

Downs, W.M. (2002), "Modeling and Behavior of the Beam/Column Joint Region of Steel Moment Resisting Frames", Ph.D. Dissertation, Virginia Tech, Virginia, USA.

Elkady, A. and Lignos, D.G. (2015), "Effect of gravity framing on the overstrength and collapse capacity of steel frame buildings with perimeter special moment frames", *Earthq. Eng. Struct. D.*, **44**(8), 1289-1307. https://doi.org/10.1002/eqe.2519.

Nunez, E., Torres, R. and Herrera, R. (2017), "Seismic performance of moment connections in steel moment frames with HSS columns", *Steel Compos. Struct.*, **25**(3), 271-286.

Fielding, D.J. and Huang, J.S. (1971), "Shear in steel beam-to-column connections", *Welding J.*, **50**(7), 313-326.

FEMA (2000), "State of the Art Report on Systems Performance of Steel Moment Frames Subject to Earthquake Ground Shaking", FEMA-355C; SAC Joint Venture, Federal Emergency Management Agency, USA.

Gupta, A. and Krawinkler, H. (1999), "Seismic demands for performance evaluation of steel moment resisting frame structures", TR 132; John A. Blume Earthquake Engineering Research Center, Stanford University, USA.

Hamburger, R.O., Krawinkler, H., Malley J.O. and Adan S.M. (2009), "Seismic design of steel special moment frames: a guide for practicing engineers', NEHRP Seismic Design Technical Brief No. 2, USA.

Krawinkler, H., Bertero, V.V. and Popov, E.P. (1971), "Inelastic

behavior of steel beam-to-column subassemblages", EERC 71-7; Earthquake Engineering Research Center, University of California, Berkeley, USA.

Krawinkler, H., Popov, E.P. and Bertero, V.V. (1975), "Shear behavior of steel frame joints", *J. Struct. Division*, **101**(11), 2317-2336.

Kawano, A. (1984), "Inelastic behavior of low-rise frame based on a weak beam-to-column connection philosophy to earthquake motion", *Proceedings of the 8th World Conference on Earthquake Engineering*, New Jersey, July

Krawinkler, H. and Mohasseb, S. (1987), "Effects of panel zone deformations on seismic response", *J. Constr. Steel Res.*, **8**, 233-250. https://doi.org/10.1016/0143-974X(87)90060-5.

Kim, K. and Engelhardt, M.D. (1995), "Development of analytical models for earthquake analysis of steel moment frames", Ph.D. Dissertation, Phil M. Ferguson Structural Engineering Laboratory, University of Texas at Austin, Texas, USA

Kim, K. and Engelhardt, M.D. (2002), "Monotonic and cyclic loading models for panel zones in steel moment frames", *J. Constr. Steel Res.*, **58**(5), 605-635. https://doi.org/10.1016/S0143-974X(01)00079-7.

Kalkan, E. and Kunnath, S.K. (2006a), "Effects of fling step and forward directivity on seismic response of buildings", *Earthq. Spectra*, **22**(2), 367-390. https://doi.org/10.1193/1.2192560.

Kalkan, E. and Kunnath, S.K. (2006b), "Adaptive modal combination procedure for nonlinear static analysis of building structures", *J. Struct. Eng.*, **132**(11), 1721-1731. https://doi.org/10.1061/(ASCE)0733-9445(2006)132:11(1721).

Kalkan, E. and Chopra, A.K. (2010), "Practical guidelines to select and scale earthquake records for nonlinear response history analysis of structures", 1068(2010); U.S. Geological Survey, USA

Lee, S.J., (1987), "Seismic Behavior of Steel Building structure with Composite Slabs", Ph.D. Thesis, Department of Civil Engineering, Lehigh University, Bethlehem, USA

Lignos, D.G., and Krawinkler, H. (2009), "Sidesway collapse of deteriorating structural systems under seismic excitations", TB 172, The John A. Blume Earthquake Engineering Research Center, Stanford University, USA.

Lignos, D.G. and Krawinkler, H. (2011), "Deterioration modeling of steel components in support of collapse prediction of steel moment frames under earthquake loading", *J. Struct. Eng.*, **137** (11), 1291-1302. https://doi.org/10.1061/(ASCE)ST.1943-541X.0000376.

Lu, L.F., Xu, Y.L., Zheng, H. and Lim, J.B. (2018a), "Cyclic response and design procedure of a weak-axis cover-plate moment connection", *Steel Compos. Struct.*, **26**(3), 329-345. https://doi.org/10.12989/scs.2018.26.3.329.

Lu, L.F., Xu, Y.L. and Lim, J.B. (2018b), "Mechanical performance of a new I-section weak-axis column bending connection", *Steel Compos. Struct.*, **26**(1), 31-44. https://doi.org/10.12989/scs.2018.26.1.031.

Lu, L.F., Xu, Y.L., Liu, J. and Lim, J.B. (2017), "Cyclic performance and design recommendations of a novel weak-axis reduced beam section connection", *Steel Compos. Struct.*, **27**(3), 337-353. https://doi.org/10.12989/scs.2017.27.3.337.

Liew, J.R. and Chen, W.F. (1995), "Analysis and design of steel frames considering panel joint deformations", *J. Struct.. Eng.*, **121**(10), 1531-1540. https://doi.org/10.1061/(ASCE)0733-9445(1995)121:10(1531).

Mckenna, F.T. (1997), "Object-oriented finite element programming: frameworks for analysis, algorithms and parallel computing", Ph.D. Dissertation, University of California, Berkeley, USA

Mansouri, I. and Saffari, H. (2014), "A new steel panel zone model including axial force for thin to thick column flanges", *Steel Compos. Struct.*, **16**(4), 417-436. https://doi.org/10.12989/scs.2014.16.4.417.

Mansouri, I. and Saffari, H. (2015), "New mathematical modeling of steel panel zone with thin to thick column flanges", *Asian J. Civil Eng. (BHRC)*, **16**(4), 451-466.

Popov, E.P. and Stephen, R.M. (1970), "Cyclic loading of full-size steel connections, UCB/EERC-70/03; Earthquake Engineering Research Center, University of California, Berkeley, USA.

Popov E.P., Amin, N., Louie. J. and Stephen, R. (1985), "Cyclic behavior of large beam-column assembles", *Earthq. Spectra*, **1**(2), 203-238.

Popov, E.P. (1987), "Panel zone flexibility in seismic moment joints", *J. Constr. Steel Res.*, **8**, 91-118.

Poursha, M., Khoshnoudian, F. and Moghadam, A. (2010), "Assessment of modal pushover analysis and conventional nonlinear static procedure with load distributions of federal emergency management agency for high-rise buildings", *Struct. Des. Tall Spec. Build.*, **19**(3), 291-308. https://doi.org/10.1002/tal.487.

Rafezy, B., Huynh, Q. and Gallart, H. (2014), "Explicit evaluation of steel panel zone stiffness using equivalent end zone (EEZ) model", SEAOC Convention, California, USA

Slutter, R.G. (1982), "Tests of Panel Zone Behavior in Beam-column-connections," 200.81.403.1; Fritz Engineering Laboratory, Lehigh University, Bethlehem, Pennsylvania, USA

Somerville, P.G. (1997), "Development of ground motion time histories for phase 2 of the FEMA/SAC steel project", SAC/BD-97/04; Structural Engineers Association of California, Applied Technology Council, California Universities for Research in Earthquake Engineering.

Saffari, H., Sarfarazi, S. and Fakhraddini, A. (2016), "A mathematical steel panel zone model for flanged cruciform columns", *Steel Compos. Struct.*, **20**(4), 851-867.

Schneider, S.P. and Amidi, A. (1998), "Seismic behavior of steel frames with deformable panel zones", *J. Struct. Eng.*, **124**(1), 35-42.

Tsai, K.C. and Popov, E.P. (1990), "Seismic panel zone design effect on elastic story drift in steel frames", *J. Struct. Eng.*, **116**(12), 3285-3301. https://doi.org/10.1061/(ASCE)0733-9445(1990)116:12(3285).

UBC 73 (1973), International conference of building officials, Uniform building code, Whittier, California, USA.

UBC 94 (1994), International conference of building officials, Uniform building code, Whittier, California, USA.

UBC 98 (1998), International conference of building officials, Uniform building code, Whittier, California, USA.

Wang, S.J. (1989), "Seismic response of steel building frames with inelastic joint deformation," Ph.D. Dissertation, Lehigh University, Bethlehem, Pennsylvania, USA.

2800 Standard (2005), Iranian Code of Practice for Seismic Resistant Design of Buildings, Iran.

CC

Appendix

In this appendix, section properties, as well as dimensions of model buildings used in this paper, are presented.

Table A1 Beam, column, doublar plate, and seismic mass for 3-story model building

Story	Columns			Girder	Doublar plate (m)		Seismic Mass (kg)
	Exterior	Interior	Gravity (Axis F)		Exterior	Interior	
1	W14x257	W14x311	W14x68	W33x118	0.0	0.0	4.78x10^5
2	W14x258	W14x312	W14x68	W30x116	0.0	0.0	4.78x10^5
3	W14x259	W14x313	W14x68	W24x68	0.0	0.0	5.17x10^5

Note: The column on the axis F is gravity column and bend about weak axis

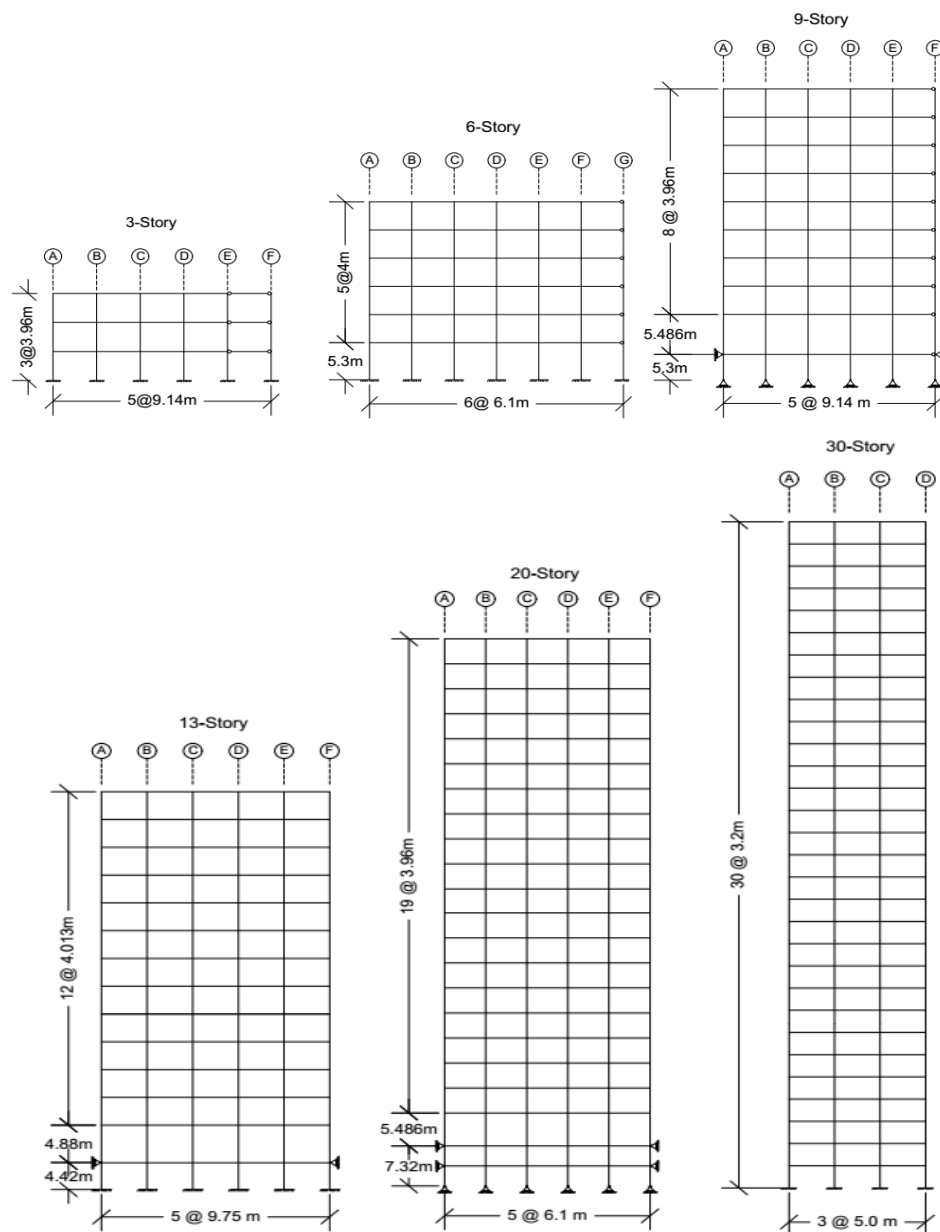The Beams between axes E and F have simple pin connections

Fig. A1: Elevations for model buildings

Table A2 Beam, column, doublar plate, and seismic mass for 6-story model building

Story	Columns		Girder	Doublar plate (m)		Seismic Mass (kg)
	Exterior	Interior		Exterior	Interior	
1	W14x176	W14x176	W30x116	0.0	0.0	2.714x10^5
2	W14x176	W14x176	W27x102	0.0	0.0	2.312x10^5
3	W14x132	W14x132	W24x68	0.0	0.0	2.312x10^5
4	W14x132	W14x132	W24x68	0.0	0.0	2.312x10^5
5	W14x90	W14x90	W24x84	0.0	0.0	2.312x10^5
6	W14x90	W14x90	W24x68	0.0	0.0	1.821x10^5

Note: The beam connections on the G axis are simple pin connections

Table A3 Beam, column, doublar plate, and seismic mass for 9-story model building

Story	Columns		Girder	Doublar plate (m)		Seismic Mass (kg)
	Exterior	Interior		Exterior	Interior	
Ground Level	W14x370	W14x500	W36x160	0.0	0.0	5.04x10^5
1	W14x370	W14x500	W36x160	0.0	0.0	4.95x10^5
2	W14x370, W14x370	W14x500, W14x455	W36x160	0.0	0.0	4.95x10^5
3	W14x370	W14x455	W36x135	0.0	0.0	4.95x10^5
4	W14x370, W14x283	W14x455, W14x370	W36x135	0.0	0.0	4.95x10^5
5	W14x283	W14x370	W36x135	0.0	0.0	4.95x10^5
6	W14x283, W14x257	W14x370, W14x283	W36x135	0.0	0.0	4.95x10^5
7	W14x257	W14x283	W30x99	0.0	0.0	4.95x10^5
8	W14x257, W14x233	W14x283, W14x257	W27x84	0.0	0.0	4.95x10^5
9	W14x233	W14x257	W24x68	0.0	0.0	5.33x10^5

Note: Column on line F bend about weak axis

Table A4 Beam, column, doublar plate, and seismic mass for 13-story model building

Story	Columns		Girder	Doublar plate (m)		Seismic Mass (kg)
	Exterior	Interior		Exterior	Interior	
Ground Level	W14x500	W14x500	W36x194	0.0	0.0	7.13x10^5
1	W14x500	W14x500	W36x230	0.0	0.0	6.81x10^5
2 ,3	W14x426	W14x426	W33x152	0.0	0.0	6.13x10^5
4,5	W14x398	W14x398	W33x152	0.0	0.0	6.13x10^5
6,7	W14x311	W14x311	W33x152	0.0	0.0	6.13x10^5
8,9	W14x283	W14x283	W33x141	0.0	0.0	6.13x10^5
10,11	W14x257	W14x257	W33x130	0.0	0.0	6.13x10^5
12	W14x159	W14x159	W33x118	0.0	0.0	6.13x10^5
13	W14x159	W14x159	W27x84	0.0	0.0	3.065x10^5

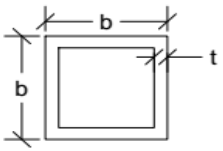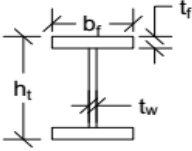Table A5 Beam, column, doublar plate, and seismic mass for 20-story model building

| Story | Columns | | Girder | Doublar plate (m) | | Seismic Mass (kg) |
	Exterior	Interior		Exterior	Interior	
Basement 1	W24x229	W24x229	W12x14	0.0	0.0	-
Ground Level	W24x229	W24x229	W30x132	0.0	0.00635	-
1	W24x229, W24x229	W24x229, W24x229	W30x132	0.0	0.00635	2.82x10^5
2	W24x229	W24x229	W30x132	0.0	0.00635	2.755x10^5
3	W24x229, W24x229	W24x229, W24x229	W30x132	0.0	0.00635	2.755x10^5
4	W24x229	W24x229	W30x132	0.0	0.00635	2.755x10^5
5	W24x229, W24x192	W24x229, W24x192	W30x132	0.0	0.0127	2.755x10^5
6	W24x192	W24x192	W30x132	0.0	0.0127	2.755x10^5
7	W24x192, W24x192	W24x192, W24x192	W30x132	0.0	0.0127	2.755x10^5
8	W24x192	W24x192	W30x116	0.0	0.00635	2.755x10^5
9	W24x192, W24x192	W24x192, W24x192	W30x116	0.0	0.00635	2.755x10^5
10	W24x192	W24x192	W27x114	0.0	0.00635	2.755x10^5
11	W24x192, W24x192	W24x192, W24x192	W27x114	0.0	0.00635	2.755x10^5
12	W24x192	W24x192	W27x94	0.0	0.00635	2.755x10^5
13	W24x192, W24x162	W24x192, W24x162	W27x94	0.0	0.00635	2.755x10^5
14	W24x162	W24x162	W27x94	0.0	0.00635	2.755x10^5
15	W24x162, W24x162	W24x162, W24x162	W27x94	0.0	0.00635	2.755x10^5
16	W24x162	W24x162	W24x62	0.0	0.0	2.755x10^5
17	W24x162, W24x131	W24x162, W24x131	W24x62	0.0	0.0	2.755x10^5
18	W24x131	W24x131	W21x57	0.0	0.0	2.755x10^5
19	W24x131, W24x131	W24x131, W24x131	W21x57	0.0	0.0	2.755x10^5
20	W24x131	W24x131	W21x57	0.0	0.0	2.92x10^5

Table A6 Beam, column, doublar plate, and seismic mass for 30-story model building

| Story | Columns (BOX b*b*t) (m) | | Girder | Doublar plate (m) | | Seismic Mass (kg) |
	Exterior	Interior		Exterior	Interior	
1 to 11	BOX 0.5 x 0.5 x 0.035	BOX 0.5 x 0.5 x 0.035	B1	0.0	0.0	5.54x10^4
12 to 14	BOX 0.45 x 0.45 x 0.03	BOX 0.5 x 0.5 x 0.035	B1	0.0	0.0	5.54x10^4
15 to 19	BOX 0.45 x 0.45 x 0.03	BOX 0.5 x 0.5 x 0.035	B2	0.0	0.0	5.54x10^4
20,21	BOX 0.45 x 0.45 x 0.03	BOX 0.45 x 0.45 x 0.03	B2	0.0	0.0	5.54x10^4
22,23	BOX 0.45 x 0.45 x 0.03	BOX 0.45 x 0.45 x 0.03	B4	0.0	0.0	5.54x10^4
24,25	BOX 0.45 x 0.45 x 0.03	BOX 0.45 x 0.45 x 0.03	B5	0.0	0.0	5.54x10^4
26,27	BOX 0.40 x 0.40 x 0.025	BOX 0.40 x 0.40 x 0.025	B5	0.0	0.0	5.54x10^4
28	BOX 0.30 x 0.30 x 0.02	BOX 0.30 x 0.30 x 0.02	B5	0.0	0.0	5.54x10^4
29	BOX 0.30 x 0.30 x 0.02	BOX 0.30 x 0.30 x 0.02	B6	0.0	0.0	5.54x10^4
30	BOX 0.25 x 0.25 x 0.015	BOX 0.25 x 0.25 x 0.015	B6	0.0	0.0	5.54x10^4

Table A7 Beam section properties for 30-story model building

Beam Section	h_t (m)	t_w (m)	b_f (m)	t_f (m)
B1	0.50	0.01	0.225	0.03
B2	0.45	0.01	0.225	0.025
B4	0.40	0.01	0.225	0.02
B5	0.35	0.008	0.225	0.02
B6	0.30	0.008	0.20	0.015